

On the possibility of a search for the $L_\mu - L_\tau$ gauge boson at Belle-II and neutrino beam experiments

Yuya Kaneta^{1,*} and Takashi Shimomura^{2,*}

¹*Graduate School of Science and Technology, Niigata University, Niigata 950-2181, Japan*

²*Faculty of Education, Miyazaki University, Miyazaki 889-2192, Japan*

*E-mail: kaneta@muse.sc.niigata-u.ac.jp, shimomura@cc.miyazaki-u.ac.jp

Received January 10, 2017; Revised March 7, 2017; Accepted March 31, 2017; Published May 18, 2017

We study the possibilities of a search for the light and weakly interacting gauge boson in the gauged $L_\mu - L_\tau$ model. Introducing the kinetic mixing at the tree level, the allowed parameter regions for the gauge coupling and kinetic mixing parameter are presented. Then, we analyze one photon plus missing event within the allowed region and show that a search for the light gauge boson will be possible at the Belle-II experiment. We also analyze the neutrino trident production process in neutrino beam experiments.

Subject Index B40, B54, B59, C31, C32

1. Introduction

The anomalous magnetic moment of the muon, $(g - 2)_\mu$, is one of the most precisely measured and calculated quantities in particle physics; it can therefore provide a sensitive search for new physics beyond the Standard Model (SM). Over recent decades, there has remained a discrepancy between experimental values [1,2] and the SM predictions [3–6],

$$\Delta a_\mu \equiv a_\mu^{\text{exp}} - a_\mu^{\text{theo}} = (28.8 \pm 8.0) \times 10^{-10}, \quad (1)$$

which corresponds to a 3.6σ deviation from the SM prediction. The discrepancy can be verified in forthcoming experiments that will reduce the uncertainties by about a factor of four [7,8]. If the discrepancy is confirmed by the experiments, it will be clear evidence of new physics beyond the SM.

On the theoretical side, many extensions of the SM have been proposed to explain this discrepancy (see Refs. [9,10] for reviews, and Ref. [11] for recent works). Among them, new $U(1)$ gauge symmetries are of particular interest since these are one of the minimal extensions of the SM. To resolve the discrepancy of $(g - 2)_\mu$ in this class of models, the simplest possibility is that muons are charged under the new symmetry while other SM particles are neutral. Then, the muon receives a contribution from the new gauge boson to its anomalous magnetic moment. For the $U(1)$ symmetry to be anomaly free, the condition, $3B = L_e + L_\mu + L_\tau$ must be satisfied, where B is the baryon number and $L_{e,\mu,\tau}$ are the flavor numbers, respectively.

Among anomaly-free $U(1)$ symmetries, the $L_\mu - L_\tau$ symmetry is particularly interesting [12–14]. Models with the $L_\mu - L_\tau$ symmetry can provide the large atmospheric mixing as the leading

Table 1. The charge assignment of the gauged $U(1)_{L_\mu - L_\tau}$ model. Here, l_μ and l_τ represent $SU(2)$ doublets, and μ_R and τ_R represent $SU(2)$ singlets of muon and tau flavors, respectively. All other SM fermions and the Higgs are singlet under this symmetry.

$U(1)_{L_\mu - L_\tau}$	$l_\mu = (\nu_\mu, \mu_L)^T$	$l_\tau = (\nu_\tau, \tau_L)^T$	μ_R	τ_R
	1	-1	1	-1

approximation, with some extensions such as adding right-handed neutrinos and new scalar particles to obtain the correct reactor angle of the lepton mixing [15–21], and these can also explain the gap in the cosmic neutrino spectrum observed by IceCube [22–25]. Furthermore, when the interactions between quarks and the gauge boson associated with the symmetry are introduced, the models can explain the anomalies reported by LHCb [26–28]. Recent studies of the model can be found for neutrino trident production processes [29,30], rare kaon decays [31], lepton flavor violations [32], and related phenomenologies [20,21,33–35]. For direct and indirect searches for such a gauge boson, new experiments are under preparation [36–38]. In the previous studies, the result of Ref. [29] showed that the gauge boson mass and the coupling constant must be lighter than 400 MeV and smaller than 10^{-3} without a kinetic mixing model. Such a light and weakly interacting gauge boson will be difficult to search for in high-energy experiments because its production cross sections and decay branching ratios are very suppressed. Therefore, high-luminosity or high-flux experiments like the Belle-II and neutrino oscillation experiments are suitable for the search for such a gauge boson.

The search for light and weakly interacting gauge bosons at the Belle-II experiment has been studied in the context of the dark photon scenario [39,40], where the SM fermions interact with the dark photon only through the kinetic mixing with the photon. On the other hand, in the studies on $L_\mu - L_\tau$ models mentioned above, the kinetic mixing at tree level is usually set to be zero by hand. Such tree-level kinetic mixing, however, is allowed by the symmetries and therefore should be considered simultaneously. In this paper, we consider a model with the gauged $U(1)_{L_\mu - L_\tau}$ symmetry in the presence of the kinetic mixing, and explore the allowed parameter space for the light and weakly interacting gauge boson. Then, we study the possibilities of searching for such a gauge boson in one-photon plus missing events at the Belle-II experiment, and in the neutrino trident production process at neutrino beam experiments.

This paper is organized as follows. In Sect. 2, we introduce the model with the gauged $U(1)_{L_\mu - L_\tau}$ symmetry, and show the relevant interactions and decay widths of the $L_\mu - L_\tau$ gauge boson. In Sect. 3, the experimental constraints and requirements to restrict the model parameters are explained. Then, in Sect. 4, we show the allowed parameter regions of the model. In Sect. 5, the possibilities of searching for the gauge boson at Belle-II and neutrino beam experiments are discussed. Section 6 is devoted to a summary and discussions.

2. Gauged $L_\mu - L_\tau$ model

We start our discussion by introducing our model. The SM is extended by adding the gauged $U(1)_{L_\mu - L_\tau}$ symmetry under which muon and tau flavor leptons are charged. The charge assignment of the symmetry is summarized in Table 1. Here, l_μ and l_τ represent $SU(2)$ doublets, and μ_R and τ_R represent $SU(2)$ singlets of muon and tau flavors, respectively. Then, the Lagrangian of the model takes the form

$$\mathcal{L} = \mathcal{L}_{\text{SM}} - V_{L_\mu - L_\tau} - \frac{1}{4} Z'_{\mu\nu} Z'^{\mu\nu} + \frac{\epsilon}{2} B_{\mu\nu} Z'^{\mu\nu} + g' Z'_\mu J_Z^\mu, \quad (2)$$

$$J_{Z'}^\mu = \bar{l}_\mu \gamma^\mu l_\mu + \bar{\mu}_R \gamma^\mu \mu_R - \bar{l}_\tau \gamma^\mu l_\tau - \bar{\tau}_R \gamma^\mu \tau_R, \quad (3)$$

where \mathcal{L}_{SM} and $V_{L_\mu-L_\tau}$ stand for the SM Lagrangian and the scalar potential responsible for the $L_\mu - L_\tau$ symmetry breaking, and Z' and B represent the gauge fields of the $U(1)_{L_\mu-L_\tau}$ and the hypercharge $U(1)_Y$, respectively. The same symbols are used for their field strengths. The gauge coupling constant and the kinetic mixing parameter are denoted as g' and ϵ , and the $U(1)_{L_\mu-L_\tau}$ current, $J_{Z'}^\mu$, is given by Eq. (3). In this work, we concentrate our discussion on the gauge sector and hence do not specify the potential $V_{L_\mu-L_\tau}$. We assume that the $L_\mu - L_\tau$ symmetry is spontaneously broken without conflicting experimental constraints such as the SM Higgs couplings to the SM gauge bosons.¹ Therefore, we treat the mass of Z' , $m_{Z'}$, as a free parameter.

After the electroweak and $L_\mu - L_\tau$ symmetries are broken down, the gauge bosons acquire the masses and their neutral components mix with each other due to the kinetic mixing. Then the interaction Lagrangian of leptons with the gauge bosons in a mass basis is obtained by diagonalizing their kinetic terms as well as mass terms. Assuming $m_{Z'}$ is much lighter than the Z boson mass, the interaction Lagrangian is given by

$$\mathcal{L}_{\text{int}} = e A_\mu J_{\text{EM}}^\mu + g_2 Z_\mu J_{\text{NC}}^\mu + Z'_\mu (e \epsilon \cos \theta_W J_{\text{EM}}^\mu + g' J_{Z'}^\mu) + \mathcal{O}(\epsilon^2), \quad (4)$$

where J_{EM}^μ and J_{NC}^μ are the electromagnetic and weak neutral currents of the SM, respectively, and e and θ_W are the electric charge and the Weinberg angle. In Eq. (4), we have neglected the terms of order ϵ^2 and higher. Such terms include the interaction of electron neutrinos with Z' . As we will show in the following sections, the kinetic mixing parameter and the gauge coupling constant of interest are smaller than 10^{-3} . Therefore, these terms can be safely ignored in our discussion. The kinetic mixing can also be generated via muon and tau loops, which is two orders of magnitude more suppressed than g' . We also ignore such a kinetic mixing for simplicity.

The decay widths of Z' are given by

$$\Gamma(Z' \rightarrow \nu \bar{\nu}) = \frac{g'^2}{24\pi} m_{Z'}, \quad (5a)$$

$$\Gamma(Z' \rightarrow e^+ e^-) = \frac{(\epsilon e \cos \theta_W)^2}{12\pi} m_{Z'} \sqrt{1 - \frac{4m_e^2}{m_{Z'}^2}} \left(1 + \frac{2m_e^2}{m_{Z'}^2}\right), \quad (5b)$$

$$\Gamma(Z' \rightarrow l^+ l^-) = \frac{(g' \mp \epsilon e \cos \theta_W)^2}{12\pi} m_{Z'} \sqrt{1 - \frac{4m_l^2}{m_{Z'}^2}} \left(1 + \frac{2m_l^2}{m_{Z'}^2}\right), \quad (5c)$$

$$\Gamma(Z' \rightarrow \text{hadrons}) = \frac{(\epsilon e \cos \theta_W)^2}{12\pi} m_{Z'} \sqrt{1 - \frac{4m_\mu^2}{m_{Z'}^2}} \left(1 + \frac{2m_\mu^2}{m_{Z'}^2}\right) R(s = m_{Z'}^2), \quad (5d)$$

where $l = \mu, \tau$, and the sign in Eq. (5c) is $-$ for μ and $+$ for τ , respectively. In Eq. (5d), $R(s)$ is the R -ratio defined by $\sigma_{e^+ e^- \rightarrow \text{hadrons}} / \sigma_{e^+ e^- \rightarrow \mu^+ \mu^-}$ and can be found in [2]. For $\sqrt{s} \lesssim 0.36$ GeV, we use the cross section for $e^+ + e^- \rightarrow \pi^+ + \pi^-$ [41,42]. The branching ratio of $Z' \rightarrow \nu + \bar{\nu}$ obtained from Eqs. (5) is used in the following analyses.

¹ This assumption can be realized when we introduce a scalar S which is singlet under the SM gauge symmetries. Such a scalar has a quartic interaction with the SM Higgs, $|S|^2 |H|^2$. However, their mixing can be very small by taking the quartic coupling small enough.

3. Experimental constraints

In this section, we explain the experimental bounds and requirements to constrain the parameters of the model, g' , ϵ , and $m_{Z'}$.

3.1. Muon anomalous magnetic moment

As mentioned in the introduction, muons receive contributions from Z' to their anomalous magnetic moment. At the one-loop level, the contribution is given by

$$\Delta a_\mu^{Z'} = \frac{(g' - \epsilon e \cos \theta_W)^2}{8\pi^2} \int_0^1 dx \frac{2m_\mu^2 x^2(1-x)}{x^2 m_\mu^2 + (1-x)m_{Z'}^2}, \quad (6)$$

where m_μ is the mass of a muon. We require the contribution Eq. (6) to be within 2σ (3σ), which leads to

$$12.8 \text{ (4.8)} \lesssim \Delta a_\mu^{Z'} \times 10^{10} \lesssim 44.8 \text{ (52.8)}. \quad (7)$$

3.2. Neutrino trident production process

The neutrino trident production process is the scattering of a muon neutrino off the Coulomb field of a nucleus (N), producing two muons in the final state, $\nu_\mu + N \rightarrow \nu_\mu + \mu^+ + \mu^- + N$. This process can occur both in the SM and in the $L_\mu - L_\tau$ model. The process offers a sensitive search for the light Z' boson, as shown in Refs. [29,30], since the SM contributions are much suppressed due to the weak interaction. Experimental search results have been reported by the CCFR [43] and CHARM-II [44] collaborations, and the most stringent bound was set by the CCFR experiment,

$$R_{CCFR} \equiv \frac{\sigma_{CCFR}}{\sigma_{SM}} = 0.82 \pm 0.28. \quad (8)$$

In Ref. [29], it was shown that the favored parameter region of $(g - 2)_\mu$ is excluded for $m_{Z'} \gtrsim 400$ MeV without the kinetic mixing in the $L_\mu - L_\tau$ model. In Sect. 4, we calculate the trident production cross section under the equivalent photon approximation [45,46] using CalcHEP [47] for the photon-neutrino scattering cross section. We found that our cross sections and results are in good agreement with Ref. [48] and Ref. [29]. We require the Z' contribution to be less than the 95% C.L. of Eq. (8).

3.3. Neutrino-electron scattering

Neutrino-electron scattering tightly constrains g' and ϵ for a dark photon and a light Z' boson [49,50]. To our model, the constraints from reactor neutrino experiments, e.g. the TEXONO experiment [51–54], are irrelevant because the interaction of electron neutrinos with Z' is negligibly small. Then, the most stringent constraints come from the Borexino experiment [55], which has measured solar neutrinos. The ${}^7\text{Be}$ neutrinos, which are ν_e , oscillate to ν_μ and ν_τ on the way to the Earth and therefore are scattered by electrons via Z' exchange. In Ref. [49], the constraint from Borexino in a $U(1)_{B-L}$ model was studied. We translate the constraint given in Ref. [49]² using

$$g_{B-L} > \left[(\epsilon e \cos \theta_W)^2 \sum_{j=1}^3 f_i |g_{ij}|^2 \right]^{1/4}, \quad (9)$$

² The constraint including the interference effect was studied in Ref. [50], which showed that the constraint is improved by about 30%. This effect is important and will be included in our next work.

$$|g_{ij}| \equiv |g'(V^\dagger Q V)_{ij}| = g' \begin{pmatrix} 0.051 & 0.158 & 0.556 \\ 0.158 & 0.082 & 0.808 \\ 0.556 & 0.808 & 0.133 \end{pmatrix}, \quad (10)$$

where V is the lepton mixing matrix [56,57] and $Q = \text{diag}(0, 1, -1)$ is the $L_\mu - L_\tau$ charge matrix; f_i stands for the fraction of i th mass eigenstate of ${}^7\text{Be}$ neutrinos at the Earth [58]. Here, we assumed the normal hierarchy of the neutrino mass spectrum [2].³

3.4. Beam dump experiment

Dark photon searches at electron beam dump experiments, such as E141 [59] and U70 [60], also restrict the model parameters. The coupling constant and kinetic mixing parameter are allowed when the Z' boson decays in a beam dump before it reaches a detector, or it is long-lived so that it penetrates a detector. The latter case corresponds to too small a coupling constant and kinetic mixing, which cannot explain $(g - 2)_\mu$. Therefore we consider the former case. The constraint can be translated from the study in the dark photon scenario [61] by

$$\frac{|\epsilon \cos \theta_W|}{\sqrt{\text{Br}(Z' \rightarrow e^+ e^-)}} \gtrsim \epsilon_{\text{BD}}, \quad (11)$$

where ϵ_{BD} is the kinetic mixing parameter for the dark photon given in [61].

3.5. Meson decay experiment

Other dark photon searches were performed at the NA48/2 [62] and E787, E949 [63,64] experiments in which the signals of the dark photon production were sought from the decays of pion and kaon, respectively. These analyzed the dark photon decay into an electron and a positron in NA48/2, and into invisible particles in E787/E949. The constraints from these experiments give similar bounds, and hence we employ the NA48/2 result.⁴ Then, the constraint can be translated using

$$|\epsilon \cos \theta_W| \sqrt{\text{Br}(Z' \rightarrow e^+ e^-)} \lesssim \epsilon_{\text{MD}}, \quad (12)$$

where ϵ_{MD} is the kinetic parameter given in Ref. [62].

3.6. Electron–positron collider experiment

The Z' boson can be directly produced in e^+e^- collisions via the kinetic mixing. Searches for a light gauge boson such as the dark photon have been performed in e^+e^- colliders [66,67], and the most stringent bound is set by the BaBar experiment [68]. The Z' boson can decay into charged leptons and be detected as $e^+ + e^- \rightarrow \gamma + l^+ + l^-$ ($l = e, \mu$). The constraint can be translated using

$$|\epsilon \cos \theta_W| \sqrt{\text{Br}(Z' \rightarrow l^+ l^-)} \lesssim \epsilon_{\text{BaBar}}, \quad (13)$$

where ϵ_{BaBar} is the kinetic mixing parameter in the dark photon given in Ref. [68]. Furthermore, the constraint for $m_{Z'} > 2m_\mu$ in the $L_\mu - L_\tau$ model without the kinetic mixing was reported in Ref. [69] by searching for the decay of Z' into muons.

³ This constraint is almost the same for the inverted hierarchy case.

⁴ The NA64 collaboration recently reported the result of the dark photon search via invisible decays [65]. This result is similar to that from the BaBar experiment, and hence we do not consider it in this paper.

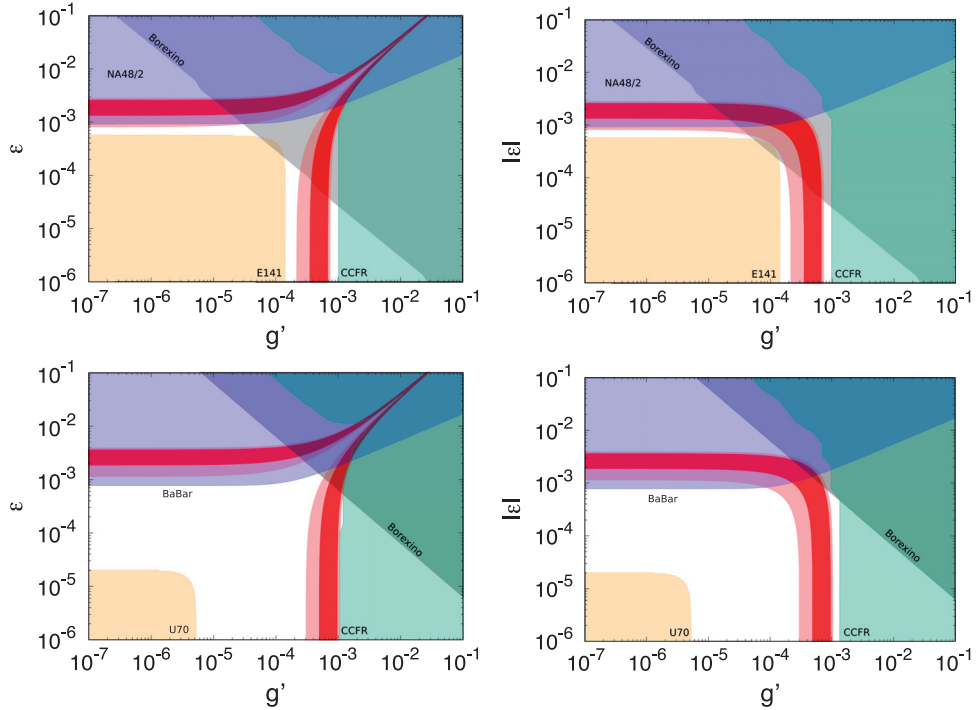


Fig. 1. The allowed region in the g' - ϵ plane. In the top and bottom panels, $m_{Z'}$ is taken as 10 and 50 MeV, respectively, and in the left and right panels, ϵ is positive and negative. The colored regions are excluded by the E141/U70 (yellow), the Borexino (gray), the CCFR (green), and $(g - 2)_e$ and/or the BaBar (blue) experiments. The red and pink bands correspond to 2σ and 3σ favored regions of $(g - 2)_\mu$.

3.7. Electron anomalous magnetic moment

The Z' boson also contributes to the magnetic moment of the electron at the one-loop level, similarly to the muon. The contribution can be obtained by simply setting $g' = 0$ and replacing m_μ with the electron mass in Eq. (6). We require that the Z' contribution to the electron magnetic moment $(g - 2)_e$ should be within 3σ [70,71],

$$\Delta a_e \lesssim 13.8 \times 10^{-13}. \quad (14)$$

4. Allowed parameter region

In this section, we show the allowed region of the parameter space in the g' - ϵ plane taking into account the constraints and requirements explained in Sect. 3. Since the constraints and requirements depend on $m_{Z'}$, we choose $m_{Z'} = 10, 50, 100$, and 300 MeV as illustrative examples.

Figure 1 shows the allowed region in the g' - ϵ plane. The mass of Z' is taken as 10 MeV and 50 MeV for the top and bottom panels, and the kinetic mixing parameter is taken to be positive and negative for the left and right panels, respectively. In the figure, the yellow, gray, and green regions are excluded by the E141/U70 (beam dump), the Borexino (ν - e scattering), and the CCFR (neutrino trident production) experiments. The blue region is also excluded by $(g - 2)_e$ and/or the BaBar (e^+e^- collider) and/or the NA48/2 (meson decay) experiment. The red and pink bands represent the favored regions of $(g - 2)_\mu$ within 2σ and 3σ , respectively. Figure 2 shows the same plots for $m_{Z'} = 100$ MeV and 300 MeV.

From these figures, one can see that the $(g - 2)_\mu$ favored regions are different with the sign of ϵ . In the case of positive ϵ (left panels), the favored region of $(g - 2)_\mu$ is extended to the upper-right

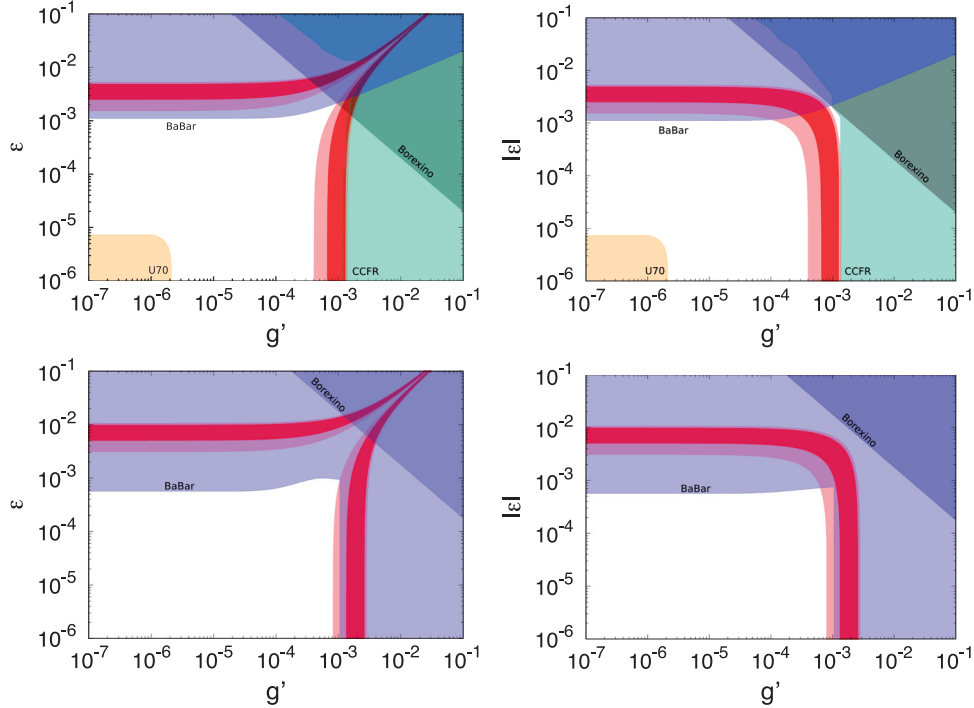


Fig. 2. As Fig. 1, for $m_{Z'} = 100 \text{ MeV}$ (top) and 300 MeV (bottom).

corner. This is because the coupling of the muon becomes smaller due to the cancellation between g' and ϵ . In this region, the constraint from the CCFR experiment can be evaded. Then, slightly larger values of g' are allowed for $m_{Z'} = 100 \text{ MeV}$. In the case of negative ϵ (right panels), on the other hand, the coupling becomes larger due to the addition of g' and ϵ . One can also see that the constraint from CCFR is more stringent in negative ϵ than in positive ϵ for $|\epsilon| \gg g'$. In this parameter region, the coupling of the muon is given by $-\epsilon e \cos \theta_W$, and therefore the relative phase of the amplitudes for the neutrino trident process is determined by the sign of ϵ . Then, the amplitudes are added destructively for positive ϵ while constructively for negative ϵ . The difference in the excluded region by CCFR comes from this fact.

It is seen that, for $g' \lesssim 10^{-4}$, the BaBar or the NA48/2 experiments exclude the regions with roughly $|\epsilon| \gtrsim 10^{-3}$ for $m_{Z'} \lesssim 100 \text{ MeV}$ and $|\epsilon| \gtrsim 5 \times 10^{-4}$ for $m_{Z'} = 300 \text{ MeV}$, respectively. Therefore, $(g - 2)_\mu$ cannot be explained within 3σ with $g' \lesssim 10^{-4}$ for $m_{Z'} \gtrsim 50 \text{ MeV}$ in our example parameters. This result generally holds for different values of $m_{Z'}$ because such a small g' does not change the constraint given in Refs. [62,68]. On the other hand, for $m_{Z'} = 10 \text{ MeV}$, the allowed region including $(g - 2)_\mu$ within 3σ is found. One will find similar allowed regions for some values of $m_{Z'} \lesssim 20 \text{ MeV}$ because the constraint from Ref. [62] becomes less stringent due to statistical fluctuations.

For $|\epsilon| \lesssim 10^{-3}$, it is seen that the regions with roughly $g' \gtrsim 10^{-3}$ are excluded by the CCFR experiment for $m_{Z'} \lesssim 100 \text{ MeV}$ and the BaBar experiment for $m_{Z'} = 300 \text{ MeV}$. For $m_{Z'} = 10 \text{ MeV}$, the E141 experiment also excludes for $g' \lesssim 1.3 \times 10^{-4}$, and the Borexino has set the upper limit on $\epsilon \lesssim 2 \times 10^{-4}$. Then, the parameter space is much constrained; however, $(g - 2)_\mu$ within 3σ is still allowed. For $m_{Z'} \gtrsim 50 \text{ MeV}$, the constraints from the beam dump experiments become weaker. These constraints come from Z' being short-lived, so that it decays before reaching a detector, as we mentioned in Sect. 3. Since the lifetime is inversely proportional to the coupling constant squared

times $m_{Z'}$, the coupling constant can be smaller as $m_{Z'}$ is larger. This $m_{Z'}$ dependence is incorporated in the values of ϵ_{BD} given in Ref. [61]. The g' and ϵ dependencies of the excluded region can be understood by Eq. (11). For $m_{Z'} = 300 \text{ MeV}$, we superposed the constraint on g' (the vertical line) read from Ref. [69]. Strictly speaking, the constraint depends on ϵ . However, it may not be so different because g' is larger than ϵ in this region.

5. Light Z' search at Belle-II and neutrino beam experiments

Based on the results shown in Sect. 4, we study the possibilities for searching for the Z' boson at the Belle-II and neutrino beam experiments.

5.1. The Belle-II experiment

The Belle-II experiment is an e^+e^- collider at the center of mass energy $\sqrt{s} = 10.58 \text{ GeV}$ [72]. Its goal is to accumulate the integrated luminosity of 50 ab^{-1} of e^+e^- collision data by the middle of the next decade. In e^+e^- collisions, the Z' boson can be produced through the kinetic mixing [73–75], and then decays into neutrinos, charged leptons, and pions. The processes with charged leptons and pions in the final states will be overwhelmed by the SM backgrounds because those can occur by electromagnetic interaction. The process with neutrinos, on the other hand, occurs by the weak interaction in the SM, and it is suppressed by the W and Z boson mass. Therefore the signal can be comparable to or larger than the background. Furthermore, the signal of the Z' production can be characterized by the energy of an associated photon.⁵ The energy of the photon is given by

$$E_\gamma = \frac{4E_{e^+}E_{e^-} - m_{Z'}^2}{2(E_{e^+} + E_{e^-} + (E_{e^+} - E_{e^-}) \cos \theta_\gamma)}, \quad (15)$$

where E_{e^\pm} is the energy of the positron and electron, and θ_γ is the angle between the photon momentum and the electron momentum. Here we ignored the angle between the positron and electron momenta for simplicity. The Belle-II detector can identify the photon for $E_\gamma \geq 0.1 \text{ GeV}$ with a resolution of 0.1 GeV and angle $15^\circ \leq \theta_\gamma \leq 135^\circ$ [72]. With these cuts, the photon energy range is $4.3 \leq E_\gamma \leq 6.9 \text{ GeV}$.

Figure 3 shows the differential cross section of $e^+ + e^- \rightarrow \gamma + Z'$ with respect to the photon energy, E_γ . The blue, green, and orange histograms correspond to $\epsilon = 2 \times 10^{-4}, 2 \times 10^{-5}$, and 6×10^{-6} , respectively. The gray histogram represents the SM background of $\gamma + \text{missing}$ events, which comes from $e^+ + e^- \rightarrow \gamma + Z^* \rightarrow \gamma + \nu + \bar{\nu}$, and also the t-channel W exchange. The mass of Z' is fixed to 100 MeV ; however, the differential cross section is almost independent of the mass for $m_{Z'} \lesssim 300 \text{ MeV}$. It can be seen from the figure that the differential cross section of the Z' production is different from the SM background. The deviations from the background become significant as ϵ becomes larger. The expected numbers of events in the last two bins are 1500, 15, and 1.4 for each ϵ , respectively, while that of the SM background is less than 1. Therefore, the search for Z' will be possible even for $\epsilon = 6 \times 10^{-6}$ by measuring the mono photon events with $E_\gamma \gtrsim 6.8 \text{ GeV}$.

Figures 4 and 5 are the contour plots of the cross section of $e^+ + e^- \rightarrow \gamma + Z'$ followed by $Z' \rightarrow \nu + \bar{\nu}$ in the $g' - \epsilon$ plane, where the decay branching ratio of $Z' \rightarrow \nu + \bar{\nu}$ is obtained from Eqs. (5). In each panel, the mass of Z' and the sign of ϵ are the same as Figs. 1 and 2, respectively. The dashed curves represent the contours of the cross section between 200 ab to 0.02 ab from top to bottom. Assuming a luminosity of 50 ab^{-1} , the expected numbers of events for each cross section

⁵ A similar search was done at BaBar for a pseudo scalar [76].

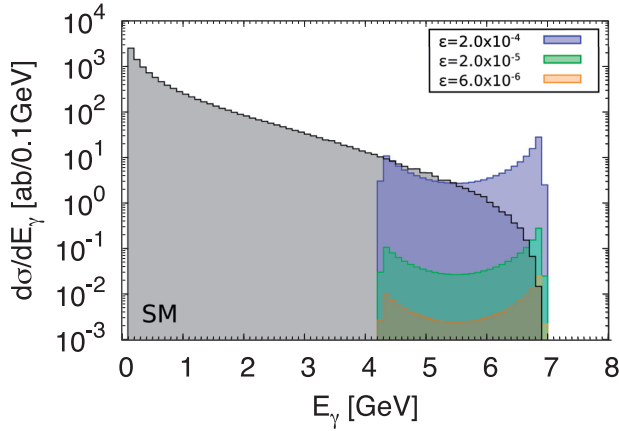


Fig. 3. The differential cross section of $e^+ + e^- \rightarrow \gamma + Z'$ with respect to the photon energy, E_γ . The blue, green, and orange histograms correspond to $\epsilon = 2 \times 10^{-4}$, 2×10^{-5} , and 6×10^{-6} , respectively. The gray histogram represents the SM background.

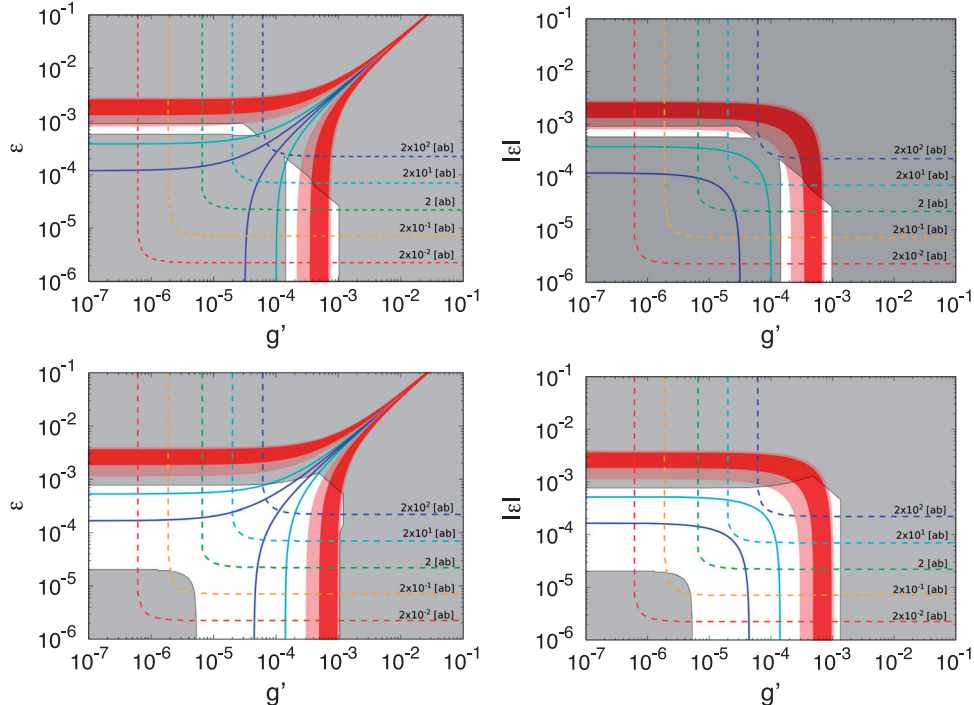


Fig. 4. Contour plots of the total cross section of $e^+ + e^- \rightarrow \gamma + \nu + \bar{\nu}$ for 10 MeV (top) and 50 MeV (bottom). The left and right panels correspond to $\epsilon > 0$ and $\epsilon < 0$, respectively. The numbers near each dashed curves are the cross sections in ab. The red and pink bands represent $(g - 2)_\mu$ within 2σ and 3σ , and the solid cyan and blue curves represent $\Delta a_\mu = 10^{-10}$ and 10^{-11} , for reference.

vary from 10^4 to 1. The gray regions are the excluded region in Figs. 1 and 2, and the red and pink bands represent the favored regions of $(g - 2)_\mu$ within 2σ and 3σ . The solid cyan and blue curves represent $\Delta a_\mu = 10^{-10}$ and 10^{-11} , for reference. When the planned experiments reduce the uncertainties, and if similar progress is made on theoretical side, such smaller contributions to $(g - 2)_\mu$ might be required.

The shape of the contours can be understood as follows. The production cross section of Z' is proportional to ϵ^2 , while the decay branching ratio is proportional to $g'^2/(g'^2 + \epsilon^2 + \dots)$. Thus, the

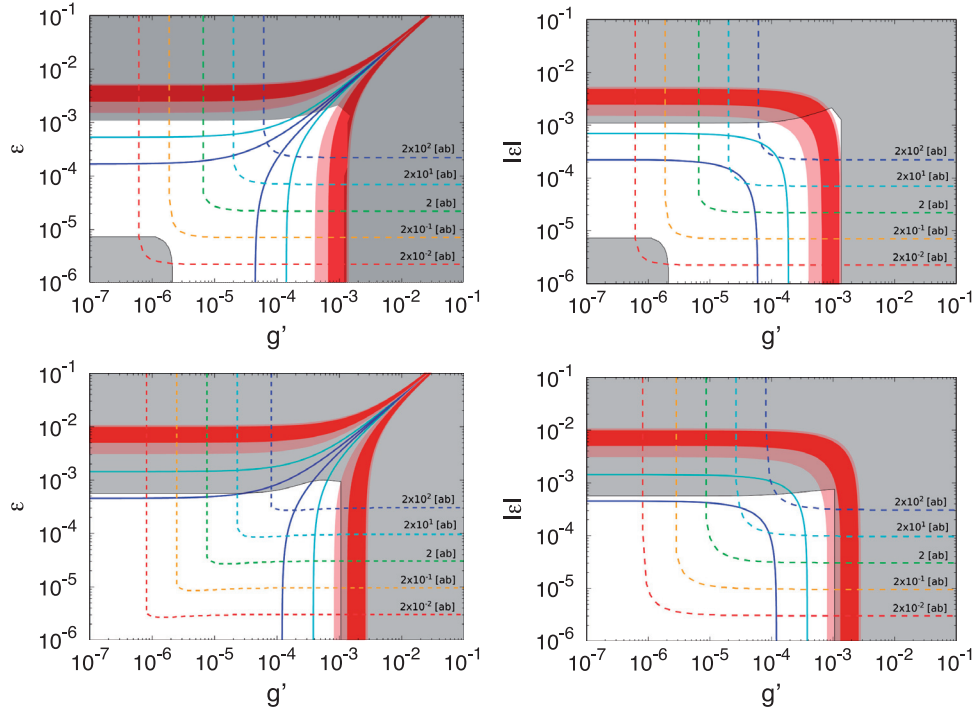


Fig. 5. As Fig. 4, for $m_{Z'} = 100$ MeV (top) and 300 MeV (bottom).

total cross section is proportional to $\epsilon^2 g'^2 / (g'^2 + \epsilon^2 + \dots)$. When ϵ is much smaller than g' , the total cross section is independent of g' . In the opposite situation, $\epsilon \gg g'$, the cross section becomes independent of ϵ . It is important to note here that the differential cross section with respect to E_γ is the same on each contour even if the branching ratio is different. This is because the shape of the different cross section is determined by the production cross section, and the magnitude of that is determined by the total cross section.

The contour of 0.2 ab is close to the case of $\epsilon = 6 \times 10^{-6}$ in Fig. 3. From Figs. 4 and 5, it can be seen that the contour of 0.2 ab covers the region of $g' \gtrsim 2 \times 10^{-6}$ and $\epsilon \gtrsim 7 \times 10^{-6}$. As discussed in Fig. 3, the signal is larger than the SM background and hence this region will be explored. Furthermore, the curves of $\Delta a_\mu = 10^{-10}$ and 10^{-11} are covered in this region. Therefore, not only the present $(g - 2)_\mu$ favored regions but also smaller ones can be examined by the Belle-II experiment.

5.2. Neutrino beam experiments

Next, we discuss the detection possibilities of the Z' boson at neutrino beam experiments through the neutrino trident production process.⁶

Figure 6 shows the cross section of the neutrino trident production (left) in the $L_\mu - L_\tau$ model and the SM, and the ratio of the cross section to the SM one, R , (right) in terms of the neutrino energy, E_ν . We assume an iron target with mass number 55.0 and the atomic number 26. The kinetic mixing parameter is fixed to $\epsilon = 10^{-5}$, and the mass is chosen as $m_{Z'} = 10$ MeV (red curves) and 100 MeV (blue curves) as reference values, respectively. The gauge coupling constant is taken to be

⁶ Some results in this subsection overlap with Ref. [30], which appeared on arXiv while our manuscript was being prepared. The results were presented at “The International Workshop on Future Potential of High Intensity Accelerators for Particle and Nuclear Physics” (HINT2016), at J-PARC, Tokai, Japan, and other places.

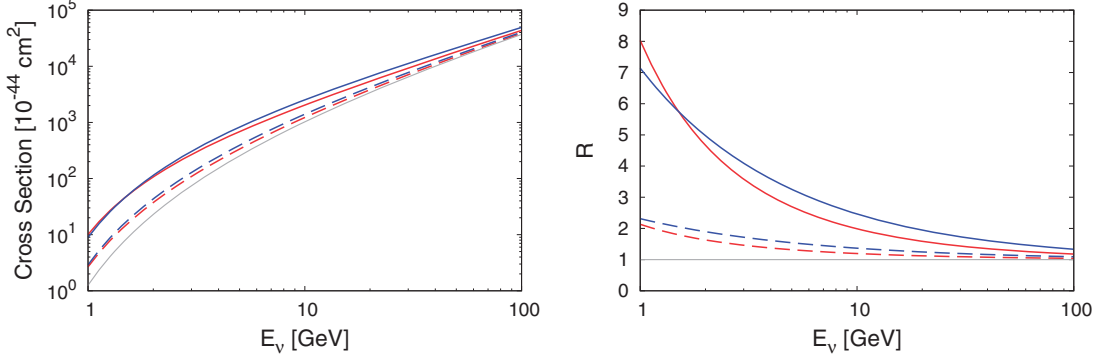


Fig. 6. The cross section of the neutrino trident production process (left) and the ratio of the cross section to the SM one, R , (right) in terms of the neutrino energy for an iron target. The kinetic mixing parameter is fixed to 10^{-5} , and the Z' mass is taken to be 10 MeV (red) and 100 MeV (blue), respectively. The gauge coupling constant is taken as $g' = 5.8 \times 10^{-4}$ (red solid), 3.4×10^{-4} (red dashed), and $g' = 9.5 \times 10^{-4}$ (blue solid), 5.8×10^{-4} (blue dashed), respectively. The gray curve represents the SM cross section.

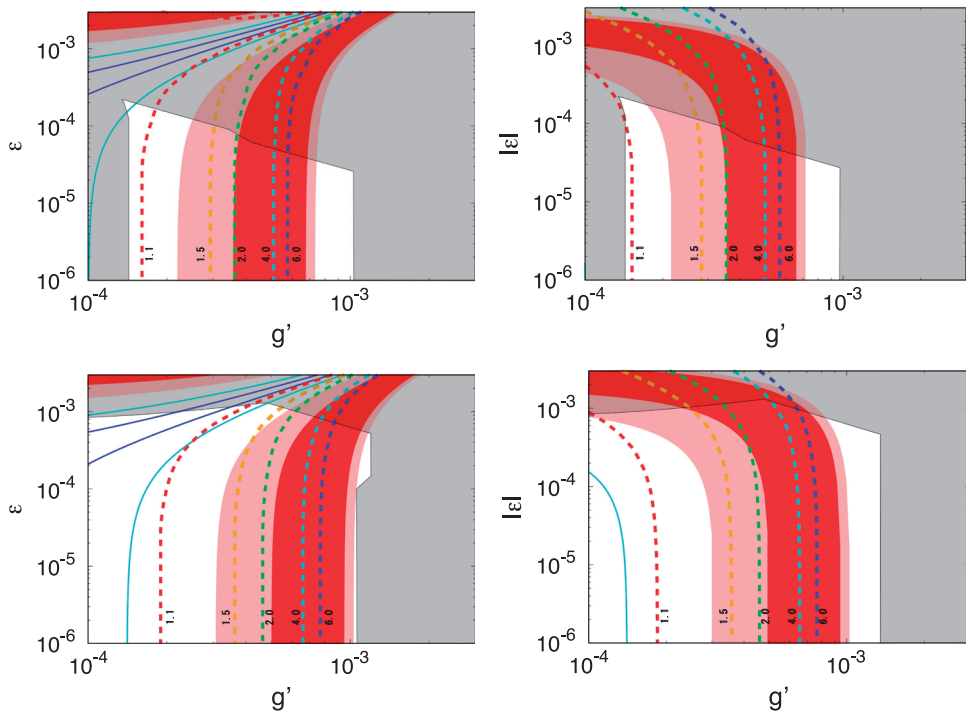


Fig. 7. Contour plot of R in the g' – ϵ plane for 10 MeV (top) and 50 MeV (bottom). The dashed curves represent R with the number indicated beside. The gray region, the red and pink bands, and the solid curves are the same as in Figs. 4 and 5.

$g' = 5.8 \times 10^{-4}$ (red solid), 3.4×10^{-4} (red dashed), and $g' = 9.5 \times 10^{-4}$ (blue solid), 5.8×10^{-4} (blue dashed), respectively. The gray curve represents the SM cross section. It can be seen from the left panel that the trident production cross section becomes larger as the neutrino energy is larger. It reaches $(3.7\text{--}4.9) \times 10^{-40}$ cm² for $E_v = 100$ GeV and $(0.12\text{--}1.0) \times 10^{-43}$ cm² at $E_v = 1$ GeV. It can also be seen from the right panel that the ratio R becomes larger as E_γ is lower. This fact suggests that neutrino beams with lower energy have better sensitivity for searching for the light Z' boson. The ratio is roughly larger than 2 for $E_v \lesssim 1.5$ GeV for our reference parameters. Since the cross

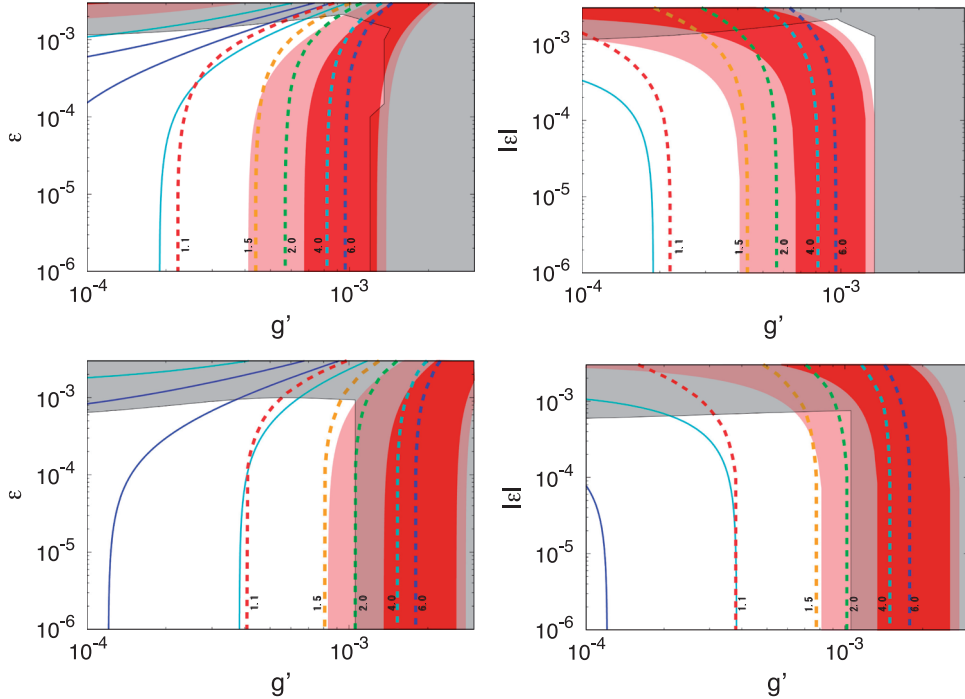


Fig. 8. As Fig. 8 for 100 MeV (top) and 300 MeV (bottom).

section becomes smaller for a lower-energy beam, larger flux is inevitably needed to have enough events. For higher neutrino energies, such as DUNE [37] and SHiP [38], the detailed study can be found in Ref. [30].

In Figs. 7 and 8, the ratios of the cross section are shown for the same parameters as Figs. 1 and 2. The values of R are indicated near each curve. The energy of the neutrino is taken to be 1.5 GeV, which is the same energy as the INGRID detector at the T2K experiment [77]. One can see that the contour curves are different in the left and right panels for each $m_{Z'}$. As explained in Sect. 4, the difference originates from the relative phase between the amplitudes, and is significant for the lower neutrino energy. In the panels, it can be seen that the region with g' smaller than from the present bound can be searched even for $R \lesssim 6$, except for $m_{Z'} = 300$ MeV. It can also be seen that the same ratio as the CCFR experiment, $R \lesssim 1.1$, can provide the search for the entire region of $(g - 2)_\mu$ within 3σ for $m_{Z'} \lesssim 300$ MeV and also some part of $\Delta a_\mu = 10^{-10}$.

As mentioned above and in Sect. 4, the Z' contribution to the trident production cross section can be positive or negative depending on ϵ . In fact, when $\epsilon > g' > 0$, the Z' amplitude is negative and interferes destructively with the SM amplitude. Then, the ratio R can become smaller than unity. This cannot happen in the $L_\mu - L_\tau$ model without the tree-level kinetic mixing because the loop-induced kinetic mixing is always smaller than g' .

Figure 9 shows the ϵ dependence of R . The mass of Z' is taken to be $m_{Z'} = 50, 100$, and 300 MeV for the dotted, dashed, and solid curves, and the coupling constant is taken to be $g' = 10^{-4}$ and 5×10^{-4} for the red and blue ones, respectively. The neutrino energy is fixed at 1.5 GeV. It can be seen that R gradually decreases as ϵ increases, and then quickly increases after it reaches a minimum. This behavior can be understood as follows. The interference term with the SM amplitude is proportional to $g' - \epsilon e \cos \theta_W$, while the absolute square of the Z' amplitude is proportional to the square of that. Therefore the total cross section decreases linearly in ϵ . After reached the minimum, the absolute

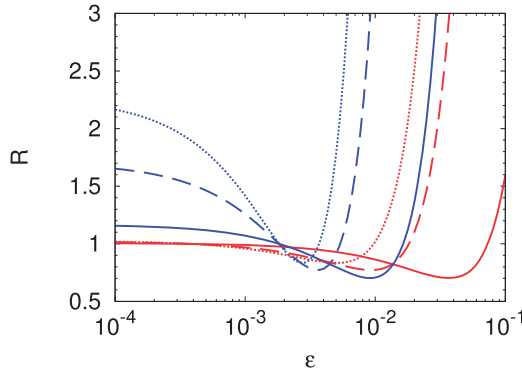


Fig. 9. The ratio of the cross sections, R , as a function of g' . The solid, dashed, and dotted curves represent R for $m_{Z'} = 300, 100$, and 50 MeV, and the red and blue ones for $g' = 10^{-4}$ and 5×10^{-4} , respectively. The neutrino energy is fixed at $E_\nu = 1.5$ GeV.

squared term dominates over the interference term and the cross section increases quadratically in ϵ . It can also be seen that ϵ at the minimum is larger as g' is smaller. Moreover, it can be seen that the minimum of R is smaller for larger $m_{Z'}$ and is independent of g' . The minimum is easily obtained by minimizing the total cross section with respect to it, and is given by $\epsilon_{\min} = \frac{1}{e \cos \theta_W} (g' + g'^{-1} \frac{A}{B})$, where A and B are independent of g' and ϵ , and determined by the Z' amplitude. Then, using ϵ_{\min} , the minimum of R is given by $R_{\min} = 1 - \frac{A^2}{\sigma_{\text{SM}} B}$, where σ_{SM} stands for the SM cross section, which is independent of g' as well as ϵ . Therefore, the minimum is determined only by $m_{Z'}$ and E_ν .

The neutrino trident production process is sensitive to the sign of ϵ for $|\epsilon| \gg g'$, while the one photon plus missing search is insensitive to it. Thus, the neutrino beam experiment can provide different information from the Belle-II experiment. For $|\epsilon| \ll g'$, the constraint becomes independent of ϵ , and hence tight bounds can be set on it. On the other hand, the production cross section of Z' at $e^+ - e^-$ colliders is proportional to ϵ^2 and hence cannot explore the small kinetic mixing region. Thus, the searches for the neutrino trident production process are complementary to the $e^+ - e^-$ collider search, and are important to the search for the light and weakly interacting gauge boson.

6. Summary and discussion

We have considered the light and weakly interacting Z' boson in the gauged $L_\mu - L_\tau$ model, simultaneously taking into account the gauge interaction and the kinetic mixing. We studied the possibilities for the search for such a Z' boson analyzing one photon plus missing (neutrinos) events at the Belle-II experiment and the neutrino trident production process at neutrino beam experiments.

We have shown the allowed region in the $g' - \epsilon$ plane for $m_{Z'} = 10, 50, 100$, and 300 MeV applying various experimental constraints and requirements. Then, the one photon plus missing events from Z' decay were analyzed in the allowed region. We showed that the differential cross section in terms of E_γ has a characteristic shape, and found that the signal can be larger than the SM background for $|\epsilon| > 6.0 \times 10^{-6}$, at least at the edge of E_γ . Thus, a search for the light Z' boson will be possible at the Belle-II experiment. We also showed the cross section for the parameter space in the $g' - \epsilon$ plane that can be explored at the Belle-II experiment.

For the neutrino trident production process, we showed that a neutrino beam with lower energy is more sensitive to the existence of Z' . Then, taking $E_\nu = 1.5$ GeV, the sensitivity was shown in the $g' - \epsilon$ plane. We found that even with the ratio $R \simeq 6$, smaller parameters than the present bound can be explored. When the trident production cross section is measured more precisely, the whole

of the $(g - 2)_\mu$ favored region can be covered. We have shown that the neutrino trident production process is also sensitive to the sign of ϵ , while the one photon plus missing search is not. Therefore both experiments will be complementary in searching for the light Z' boson.

Before closing, two comments are in order: (1) For the search at Belle-II, $e^+ + e^- \rightarrow \text{multi-}\gamma$ can also be serious backgrounds if several photons are undetected. The total cross sections of two-, three-, and four-gamma final states are roughly estimated as 10^9 , 10^8 , and 10^6 ab, respectively. Thus, the expected numbers of these backgrounds would be much larger than that of the signal events. For two photons in the final state, changing the cut on the photon angle will reduce this background. However, for cases with more photons, it is not easy to reduce such events, especially for the cases where only one photon is measured and the other photons escape to beam directions. Therefore, more detailed study on the background is needed to determine the parameter space to be explored. (2) For the neutrino trident production process, the momenta and angle distributions of the muons are important to discriminate the signal from the background. We leave these for our future work.

Acknowledgements

The authors would like to thank K. Hayasaka and T. Yoshinobu for fruitful discussions and useful information on the Belle-II detector. Y. K. would like to thank the visitor support program in the Japan Particle and Nuclear Forum. The work of T. S. is supported by JSPS KAKENHI Grant no. 15K17654.

Funding

Open Access funding: SCOAP³.

References

- [1] G. W. Bennett et al. [Muon g-2Collaboration], Phys. Rev. D **73**, 072003 (2006) [[arXiv:hep-ex/0602035](#)] [[Search INSPIRE](#)].
- [2] C. Patrignani et al. [Particle Data GroupCollaboration], Chin. Phys. C **40**, 100001 (2016).
- [3] M. Davier, A. Hoecker, B. Malaescu, and Z. Zhang, Eur. Phys. J. C **71**, 1515 (2011); 72, 1874 (2012) [erratum] [[arXiv:1010.4180](#) [hep-ph]] [[Search INSPIRE](#)].
- [4] F. Jegerlehner and R. Szafron, Eur. Phys. J. C **71**, 1632 (2011) [[arXiv:1101.2872](#) [hep-ph]] [[Search INSPIRE](#)].
- [5] K. Hagiwara, R. Liao, A. D. Martin, D. Nomura, and T. Teubner, J. Phys. G **38**, 085003 (2011) [[arXiv:1105.3149](#) [hep-ph]] [[Search INSPIRE](#)].
- [6] T. Aoyama, M. Hayakawa, T. Kinoshita, and M. Nio, Phys. Rev. Lett. **109**, 111808 (2012) [[arXiv:1205.5370](#) [hep-ph]] [[Search INSPIRE](#)].
- [7] M. Aoki et al., <http://g-2.kek.jp/portal/index.html>.
- [8] J. Grange et al. [Muon g-2Collaboration], [arXiv:1501.06858](#) [physics.ins-det] [[Search INSPIRE](#)].
- [9] F. Jegerlehner and A. Nyffeler, Phys. Rep. **477**, 1 (2009) [[arXiv:0902.3360](#) [hep-ph]] [[Search INSPIRE](#)].
- [10] M. Lindner, M. Platscher, and F. S. Queiroz, [arXiv:1610.06587](#) [hep-ph] [[Search INSPIRE](#)].
- [11] P. Fayet, [arXiv:1611.05357](#) [hep-ph] [[Search INSPIRE](#)].
- [12] R. Foot, Mod. Phys. Lett. A **6**, 527 (1991).
- [13] R. Foot, X. G. He, H. Lew, and R. R. Volkas, Phys. Rev. D **50**, 4571 (1994) [[arXiv:hep-ph/9401250](#)] [[Search INSPIRE](#)].
- [14] X.-G. He, G. C. Joshi, H. Lew, and R. R. Volkas, Phys. Rev. D **44**, 2118 (1991).
- [15] S. Choubey and W. Rodejohann, Eur. Phys. J. C **40**, 259 (2005) [[arXiv:hep-ph/0411190](#)] [[Search INSPIRE](#)].
- [16] T. Ota and W. Rodejohann, Phys. Lett. B **639**, 322 (2006) [[arXiv:hep-ph/0605231](#)] [[Search INSPIRE](#)].
- [17] J. Heeck and W. Rodejohann, J. Phys. G **38**, 085005 (2011a) [[arXiv:1007.2655](#) [hep-ph]] [[Search INSPIRE](#)].
- [18] J. Heeck and W. Rodejohann, Phys. Rev. D **84**, 075007 (2011b) [[arXiv:1107.5238](#) [hep-ph]] [[Search INSPIRE](#)].

- [19] J. Heeck, M. Holthausen, W. Rodejohann, and Y. Shimizu, Nucl. Phys. B **896**, 281 (2015) [[arXiv:1412.3671](https://arxiv.org/abs/1412.3671) [hep-ph]] [[Search INSPIRE](#)].
- [20] A. Biswas, S. Choubey, and S. Khan, [arXiv:1612.03067](https://arxiv.org/abs/1612.03067) [hep-ph] [[Search INSPIRE](#)].
- [21] A. Biswas, S. Choubey, and S. Khan, J. High Energy Phys. **09**, 147 (2016b) [[arXiv:1608.04194](https://arxiv.org/abs/1608.04194) [hep-ph]] [[Search INSPIRE](#)].
- [22] M. G. Aartsen et al. [IceCubeCollaboration], Phys. Rev. Lett. **113**, 101101 (2014) [[arXiv:1405.5303](https://arxiv.org/abs/1405.5303) [astro-ph.HE]] [[Search INSPIRE](#)].
- [23] T. Araki, F. Kaneko, Y. Konishi, T. Ota, J. Sato, and T. Shimomura, Phys. Rev. D **91**, 037301 (2015) [[arXiv:1409.4180](https://arxiv.org/abs/1409.4180) [hep-ph]] [[Search INSPIRE](#)].
- [24] A. Kamada and H.-B. Yu, Phys. Rev. D **92**, 113004 (2015) [[arXiv:1504.00711](https://arxiv.org/abs/1504.00711) [hep-ph]] [[Search INSPIRE](#)].
- [25] T. Araki, F. Kaneko, T. Ota, J. Sato, and T. Shimomura, Phys. Rev. D **93**, 013014 (2016) [[arXiv:1508.07471](https://arxiv.org/abs/1508.07471) [hep-ph]] [[Search INSPIRE](#)].
- [26] W. Altmannshofer, S. Gori, M. Pospelov, and I. Yavin, Phys. Rev. D **89**, 095033 (2014a) [[arXiv:1403.1269](https://arxiv.org/abs/1403.1269) [hep-ph]] [[Search INSPIRE](#)].
- [27] W. Altmannshofer and I. Yavin, Phys. Rev. D **92**, 075022 (2015) [[arXiv:1508.07009](https://arxiv.org/abs/1508.07009) [hep-ph]] [[Search INSPIRE](#)].
- [28] W. Altmannshofer, S. Gori, S. Profumo, and F. S. Queiroz, J. High Energy Phys. **12**, 106 (2016a) [[arXiv:1609.04026](https://arxiv.org/abs/1609.04026) [hep-ph]] [[Search INSPIRE](#)].
- [29] W. Altmannshofer, S. Gori, M. Pospelov, and I. Yavin, Phys. Rev. Lett. **113**, 091801 (2014b) [[arXiv:1406.2332](https://arxiv.org/abs/1406.2332) [hep-ph]] [[Search INSPIRE](#)].
- [30] G. Magill and R. Plestid, [arXiv:1612.05642](https://arxiv.org/abs/1612.05642) [hep-ph] [[Search INSPIRE](#)].
- [31] M. Ibe, W. Nakano, and M. Suzuki, [arXiv:1611.08460](https://arxiv.org/abs/1611.08460) [hep-ph] [[Search INSPIRE](#)].
- [32] W. Altmannshofer, C.-Y. Chen, P. S. Bhupal Dev, and A. Soni, Phys. Lett. B **762**, 389 (2016b) [[arXiv:1607.06832](https://arxiv.org/abs/1607.06832) [hep-ph]] [[Search INSPIRE](#)].
- [33] K. Harigaya, T. Igari, M. M. Nojiri, M. Takeuchi, and K. Tobe, J. High Energy Phys. **03**, 105 (2014) [[arXiv:1311.0870](https://arxiv.org/abs/1311.0870) [hep-ph]] [[Search INSPIRE](#)].
- [34] S. Patra, S. Rao, N. Sahoo, and N. Sahu, [arXiv:1607.04046](https://arxiv.org/abs/1607.04046) [hep-ph] [[Search INSPIRE](#)].
- [35] J. Heeck, [arXiv:1610.07623](https://arxiv.org/abs/1610.07623) [hep-ph] [[Search INSPIRE](#)].
- [36] S. N. Gninenko, N. V. Krasnikov, and V. A. Matveev, Phys. Rev. D **91**, 095015 (2015) [[arXiv:1412.1400](https://arxiv.org/abs/1412.1400) [hep-ph]] [[Search INSPIRE](#)].
- [37] R. Acciarri et al. [DUNECollaboration], [arXiv:1512.06148](https://arxiv.org/abs/1512.06148) [physics.ins-det] [[Search INSPIRE](#)].
- [38] M. Anelli et al. [SHiPCollaboration], [arXiv:1504.04956](https://arxiv.org/abs/1504.04956) [physics.ins-det] [[Search INSPIRE](#)].
- [39] R. Essig, P. Schuster, and N. Toro, Phys. Rev. D **80**, 015003 (2009) [[arXiv:0903.3941](https://arxiv.org/abs/0903.3941) [hep-ph]] [[Search INSPIRE](#)].
- [40] R. Essig, J. Mardon, M. Papucci, T. Volansky, and Y.-M. Zhong, J. High Energy Phys. **11**, 167 (2013a) [[arXiv:1309.5084](https://arxiv.org/abs/1309.5084) [hep-ph]] [[Search INSPIRE](#)].
- [41] V. V. Ezhela, S. B. Lugovsky, and O. V. Zenin, [arXiv:hep-ph/0312114](https://arxiv.org/abs/hep-ph/0312114) [[Search INSPIRE](#)].
- [42] M. Davier, S. Eidelman, A. Hocker, and Z. Zhang, Eur. Phys. J. C **27**, 497 (2003) [[arXiv:hep-ph/0208177](https://arxiv.org/abs/hep-ph/0208177)] [[Search INSPIRE](#)].
- [43] S. R. Mishra et al. [CCFRCollaboration], Phys. Rev. Lett. **66**, 3117 (1991).
- [44] D. Geiregat et al. [CHARM-IICollaboration], Phys. Lett. B **245**, 271 (1990).
- [45] C. F. von Weizsäcker, Z. Phys. **88**, 612 (1934).
- [46] E. J. Williams, Phys. Rev. **45**, 729 (1934).
- [47] A. Belyaev, N. D. Christensen, and A. Pukhov, Comput. Phys. Commun. **184**, 1729 (2013) [[arXiv:1207.6082](https://arxiv.org/abs/1207.6082) [hep-ph]] [[Search INSPIRE](#)].
- [48] R. W. Brown, R. H. Hobbs, J. Smith, and N. Stanko, Phys. Rev. D **6**, 3273 (1972).
- [49] R. Harnik, J. Kopp, and P. A. N. Machado, J. Cosmol. Astropart. Phys. **1207**, 026 (2012) [[arXiv:1202.6073](https://arxiv.org/abs/1202.6073) [hep-ph]] [[Search INSPIRE](#)].
- [50] S. Bilmis, I. Turan, T. M. Aliev, M. Deniz, L. Singh, and H. T. Wong, Phys. Rev. D **92**, 033009 (2015) [[arXiv:1502.07763](https://arxiv.org/abs/1502.07763) [hep-ph]] [[Search INSPIRE](#)].
- [51] M. Deniz et al. [TEXONOCollaboration], Phys. Rev. D **81**, 072001 (2010) [[arXiv:0911.1597](https://arxiv.org/abs/0911.1597) [hep-ex]] [[Search INSPIRE](#)].
- [52] H. B. Li et al. [TEXONOCollaboration], Phys. Rev. Lett. **90**, 131802 (2003) [[arXiv:hep-ex/0212003](https://arxiv.org/abs/hep-ex/0212003)] [[Search INSPIRE](#)].

- [53] H. T. Wong et al. [TEXONOCollaboration], Phys. Rev. D **75**, 012001 (2007) [[arXiv:hep-ex/0605006](https://arxiv.org/abs/hep-ex/0605006)] [[Search INSPIRE](#)].
- [54] J.-W. Chen, H.-C. Chi, H.-B. Li, C. P. Liu, L. Singh, H. T. Wong, C.-L. Wu, and C.-P. Wu, Phys. Rev. D **90**, 011301 (2014) [[arXiv:1405.7168](https://arxiv.org/abs/1405.7168) [hep-ph]] [[Search INSPIRE](#)].
- [55] G. Bellini et al. [Borexino], Phys. Rev. Lett. **107**, 141302 (2011) [[arXiv:1104.1816](https://arxiv.org/abs/1104.1816) [hep-ex]] [[Search INSPIRE](#)].
- [56] Z. Maki, M. Nakagawa, and S. Sakata, Prog. Theor. Phys. **28**, 870 (1962).
- [57] B. Pontecorvo, Sov. Phys. JETP **26**, 984 (1968) [Zh. Eksp. Teor. Fiz. **53**, 1717 (1967)].
- [58] H. Nunokawa, S. J. Parke, and R. Zukanovich Funchal, Phys. Rev. D **74**, 013006 (2006) [[arXiv:hep-ph/0601198](https://arxiv.org/abs/hep-ph/0601198)] [[Search INSPIRE](#)].
- [59] E. M. Riordan et al., Phys. Rev. Lett. **59**, 755 (1987).
- [60] J. Blumlein and J. Brunner, Phys. Lett. B **701**, 155 (2011) [[arXiv:1104.2747](https://arxiv.org/abs/1104.2747) [hep-ex]] [[Search INSPIRE](#)].
- [61] R. Essig et al., Proc. Community Summer Study 2013: Snowmass on the Mississippi (CSS2013) (2013b) [[arXiv:1311.0029](https://arxiv.org/abs/1311.0029) [hep-ph]] [[Search INSPIRE](#)].
- [62] J. R. Batley et al. [NA48/2Collaboration], Phys. Lett. B **746**, 178 (2015) [[arXiv:1504.00607](https://arxiv.org/abs/1504.00607) [hep-ex]] [[Search INSPIRE](#)].
- [63] S. Adler et al. [E787Collaboration], Phys. Rev. D **70**, 037102 (2004) [[arXiv:hep-ex/0403034](https://arxiv.org/abs/hep-ex/0403034)] [[Search INSPIRE](#)].
- [64] A. V. Artamonov et al. [E949Collaboration], Phys. Rev. Lett. **101**, 191802 (2008) [[arXiv:0808.2459](https://arxiv.org/abs/0808.2459) [hep-ex]] [[Search INSPIRE](#)].
- [65] D. Banerjee et al. [NA64Collaboration] (2016) [arXiv:1610.02988](https://arxiv.org/abs/1610.02988) [hep-ph] [[Search INSPIRE](#)].
- [66] D. Babusci et al. [KLOE-2Collaboration], Phys. Lett. B **720**, 111 (2013) [[arXiv:1210.3927](https://arxiv.org/abs/1210.3927) [hep-ex]] [[Search INSPIRE](#)].
- [67] D. Babusci et al. [KLOE-2Collaboration], Phys. Lett. B **736**, 459 (2014) [[arXiv:1404.7772](https://arxiv.org/abs/1404.7772) [hep-ex]] [[Search INSPIRE](#)].
- [68] J. P. Lees et al. [BaBarCollaboration], Phys. Rev. Lett. **113**, 201801 (2014) [[arXiv:1406.2980](https://arxiv.org/abs/1406.2980) [hep-ex]] [[Search INSPIRE](#)].
- [69] J. P. Lees et al. [BaBarCollaboration], Phys. Rev. D **94**, 011102 (2016) [[arXiv:1606.03501](https://arxiv.org/abs/1606.03501) [hep-ex]] [[Search INSPIRE](#)].
- [70] G. F. Giudice, P. Paradisi, and M. Passera, J. High Energy Phys. **11**, 113 (2012) [[arXiv:1208.6583](https://arxiv.org/abs/1208.6583) [hep-ph]] [[Search INSPIRE](#)].
- [71] T. Aoyama, M. Hayakawa, T. Kinoshita, and M. Nio, Phys. Rev. D **91**, 033006 (2015) [[arXiv:1412.8284](https://arxiv.org/abs/1412.8284) [hep-ph]] [[Search INSPIRE](#)].
- [72] T. Abe et al. [Belle-IIICollaboration] (2010), [arXiv:1011.0352](https://arxiv.org/abs/1011.0352) [physics.ins-det] [[Search INSPIRE](#)].
- [73] E. Ma and J. Okada, Phys. Rev. Lett. **41**, 287 (1978); **41**, 1759 (1978) [erratum].
- [74] M. Carena, A. de Gouvea, A. Freitas, and M. Schmitt, Phys. Rev. D **68**, 113007 (2003) [[arXiv:hep-ph/0308053](https://arxiv.org/abs/hep-ph/0308053)] [[Search INSPIRE](#)].
- [75] P. Fayet, Phys. Rev. D **75**, 115017 (2007) [[arXiv:hep-ph/0702176](https://arxiv.org/abs/hep-ph/0702176)] [[Search INSPIRE](#)].
- [76] B. Aubert et al. [BaBarCollaboration], Proc. 34th Int. Conf. on High Energy Physics (ICHEP 2008) (2008) [[arXiv:0808.0017](https://arxiv.org/abs/0808.0017) [hep-ex]] [[Search INSPIRE](#)].
- [77] K. Abe et al. [T2KCollaboration], Nucl. Instrum. Meth. A **659**, 106 (2011) [[arXiv:1106.1238](https://arxiv.org/abs/1106.1238) [physics.ins-det]] [[Search INSPIRE](#)].